Fast Time-domain Impedance Spectroscopy of Lithium-ion Batteries using Pulse Perturbation

Alan G. Li*, Youssef A. Fahmy*, Melissa M. Wu†, and Matthias Preindl*
* Department of Electrical Engineering, Columbia University, New York, NY, USA
† Department of Statistics, Columbia University, New York, NY, USA
Email: matthias.preindl@columbia.edu

***Abstract*—Electrochemical impedance spectroscopy (EIS) is a useful diagnostics technique for lithium-ion batteries but measurements can last several hours. Fast pulse impedance spectroscopy (PIS) is thus proposed using just 2 minutes of pulse perturbation data and classic signal processing techniques. The method is verified using experimental data collected from 6 lithium-ion cells aged under different temperatures and charging levels. Results show that PIS can extract high-quality Nyquist plots for overpotential analysis. Comparison is made between the frequency- and time-domains using the Randles and convolution-defined diffusion equivalent circuit models. PIS is a practical time-domain impedance spectroscopy method that experimentally links EIS and convolution-defined diffusion.**

***Index Terms*—Lithium batteries, Frequency analysis, impedance spectroscopy, pulse perturbation**

I. INTRODUCTION

Lithium-ion batteries (LIBs) are important energy storage technologies for decarbonizing transport and facilitating the integration of renewable energy into the grid [1], [2]. Better management of battery degradation can reduce costs and increase useful life. Degradation of LIB cells results from complex interactions between the electrodes, electrolyte, and lithium ions that reduce maximum capacity and power output. Understanding how these mechanisms of degradation change in real time is an ongoing challenge. Health estimation and impedance characterization is thus an important task for battery management systems [3], [4]

Electrochemical impedance spectroscopy (EIS) is a popular diagnostics method [5]–[8] performed in the frequency-domain by stimulating a battery cell at frequencies ranging from mHz to kHz. The frequency-varying impedance is then used to fit a frequency-domain equivalent circuit model (ECM), shown in Fig. 1, known as the Randles circuit. The circuit is comprised of a resistor, one resistor-capacitor (RC) pair, and the Warburg impedance A_W, which captures the effects of lithium-ion diffusion. Since diffusion dynamics are influenced by degradation, EIS is a popular diagnostics tool [9], [10]. Its diagnostics time can last several hours for a single cell, however, making EIS infeasible for real-time use.

In contrast, overpotential ECMs such as the convolution-defined diffusion (CDD) model shown in Fig. 1b can be used in real time. This model introduces a CDD parameter A_D that captures diffusion like the Warburg impedance. Unlike A_W, A_D can be used in the time-domain without any fractional calculus [11]. This greatly simplifies analysis and reduces computational complexity. It is theoretically understood that A_D and A_W are linked by their ability to capture the diffusion overpotential. This is qualitatively shown in [11] but an explicit link between has not been experimentally demonstrated.

Pulse injection is a widely-used method described as early as [12] for obtaining kinetic parameters of an electrode system, but [13] is often credited today for standardizing the hybrid-pulse power characterization test for identifying ECM parameters. Pulses are powerful characterization methods because the LIB cell response to a pulse is governed by its electrochemical parameters; indeed, the relaxation response is composed of a rich interplay of ohmic, charge-transfer, and diffusion overpotentials in the solid and liquid phases [14]. Though pulses are traditionally viewed as disruptive diagnostics signals with long rest times, more advanced processing techniques could be used to increase the characterization capabilities of pulses and reduce the need for long diagnostics time [4]. This could make pulses easier to implement in real systems.

We examine a fast implementation of time-domain impedance spectroscopy from pulse perturbation of LIB cells, which we name pulse impedance spectroscopy (PIS). PIS is assessed at hundreds of unique states by inspecting the observed impedance Nyquist plots and comparing the fitted Randles parameters with the CDD parameters. It is shown that the frequency-varying impedance can be extracted using just a few minutes of pulse perturbation data. The results also demonstrate, for the first time, an experimental link between the CDD parameter A_D and the Warburg impedance A_W.

We continue in Section II to outline the theoretical concepts underpinning PIS. In Section III we describe our methodology for evaluating PIS. Results are presented and discussed in Section IV. We conclude and offer an outlook in Section V.

II. PULSE IMPEDANCE SPECTROSCOPY

A. Theoretical concepts

Pulses are known to excite a wide range of frequencies. This parallels traditional EIS, where the frequency-varying impedance is measured using sinusoidal inputs that are directly injected into the LIB cell. It is argued in [15], [16] that pulses fail to excite high-frequency components sufficiently and 'pulse-multisine' signals are proposed. Convolving a mutisine spectrum onto the pulse, however, may be infeasible outside of laboratory conditions. Thus standard pulses have been used for time-domain EIS (TD-EIS).

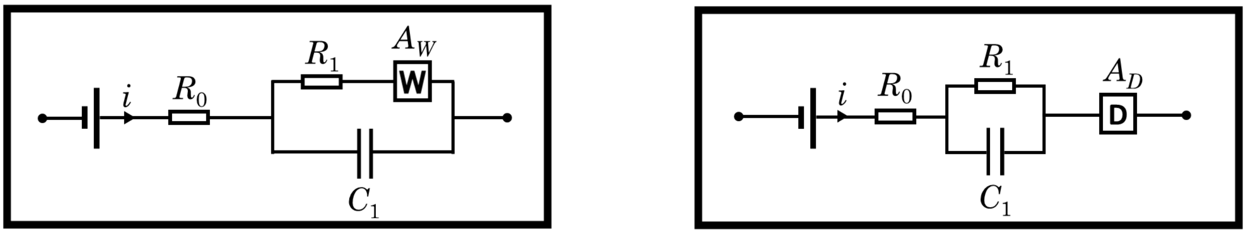

(a)

(b)

Fig. 1. Equivalent circuit models, showing (a) Randles circuit for modelling frequency-domain data and (b) convolution-defined diffusion model for time-domain overpotentials

TD-EIS is founded on digital signal processing and Fourier theory. It uses time-domain data, such as a pulse perturbation, to recover the complex frequency-varying impedance $Z(s)$, where $s = j2\pi f$ and f is the frequency. In TD-EIS, several processing steps are required to transform time-domain data to the frequency-domain [17], [18]. In [17], TD-EIS is explored with rectangle, Gaussian, and sinc pulses. Though full Nyquist curves are recovered, 20 min are required for a rectangle pulse. Drive cycle data is used in [18] using novel parameter estimation techniques. While forgoing a diagnostics signal may allow for 'passive' EIS, [18] shows that mHz characteristics are not reliably observed during drive cycles.

Fast PIS is a type of TD-EIS that aims to cover the full frequency spectrum without sacrificing speed or ease of implementation. It uses a short rectangle pulse to facilitate practical use and capture low frequencies without requiring long diagnostics times.

B. Procedure

PIS procedure follows similar steps to those in [17], [18] but fast PIS uses a rectangle pulse lasting only 2 minutes. Prior to obtaining the frequency spectrum, the time domain data is processed. First, the current and voltage harmonic components are obtained by removing the average value. A Hamming window is applied to the data to reduce spectral leakage. Finally, a 1st-order low-pass Butterworth filter of width 1 Hz is used to avoid aliasing and attenuate high frequencies.

After time-domain processing, the Fast Fourier transform is calculated for each pulse current and voltage. Since a rectangle pulse has a sinc spectrum, the components vector is sparsified by extracting only the maxima of the magnitude response. The impedance is then calculated using the ratio of the complex amplitudes of the voltage and current spectra.

$$Z(s) = \frac{V(s)}{I(s)} \tag{1}$$

Finally, a Savitzky-Golay smoothing filter [19] is applied to the real and imaginary parts of the impedance to remove fluctuations in the frequency spectrum.

Like traditional EIS, PIS uses the Nyquist plot to visualize the results. Nyquist plots are a highly distinct characterization curve where the imaginary impedance component is plotted against the real. Nyquist curves are popular for their easily-observed features, such as the high-frequency (kHz) real-axis crossing, the mid-frequency semicircle width, and the low-frequency (mHz) tail. In LIB cells, the high-, mid-, and low-range features are linked to dynamics from the solution, charge-transfer, and diffusion overpotentials [6].

The frequency-varying impedance is fitted with the Warburg-1RC Randles model,

$$\hat{Z}(s) = R_0 + \frac{R_1 + Z_W}{1 + sR_1C_1 + sZ_WC_1} \tag{2}$$

where R_0 is the ohmic resistance and the Warburg impedance Z_W is defined as

$$Z_W(s) = \frac{A_W}{\sqrt{s}} \tag{3}$$

where A_W is the Warburg constant, inverse-square proportional to the aggregated semi-infinite diffusion coefficient D of lithium-ions in the cell [20]–[22]

$$\frac{1}{A_W} = \frac{F^2\bar{c}_i\sqrt{D}}{RT} \tag{4}$$

where F is Faraday's constant, $\bar{c}_i$ is average concentration of lithium, R is the gas constant, and T is the temperature. Parameter identification is performed using scatter-search global optimization,

$$\begin{aligned} \text{minimize} \quad & \|r\|_2^2 \\ r(s) &= Z(s) - \hat{Z}(s,\theta) \\ \theta &= (R_0 \quad R_1 \quad C_1 \quad A_W)^T \end{aligned} \tag{5}$$

where $\|r\|_2^2$ is the sum of the squared residuals.

III. METHODOLOGY

A. Data Collection

We assess fast PIS using cell data collected at a wide range of states. Six nickel-magnesium-cobalt Panasonic NCR18650PF cells were cycled using two stress factors applied to three cells each. In stress factor 1 (S1), cells were degraded at low state of charge (SoC) (0 to 0.5) and low temperature (8°C), while in stress factor 2 (S2) cells were degraded at high SoC (0.5 to 1) and high temperature (40°C). All cells were cycled 2.7 A, corresponding to 1 C-rate. These two types of stress factors have different effects on how the cell state of health (SoH) changes over time [23], [24].

Pulses were 2 min long, with an amplitude of 2.7 A and split equally between charge-rest and discharge-rest portions.

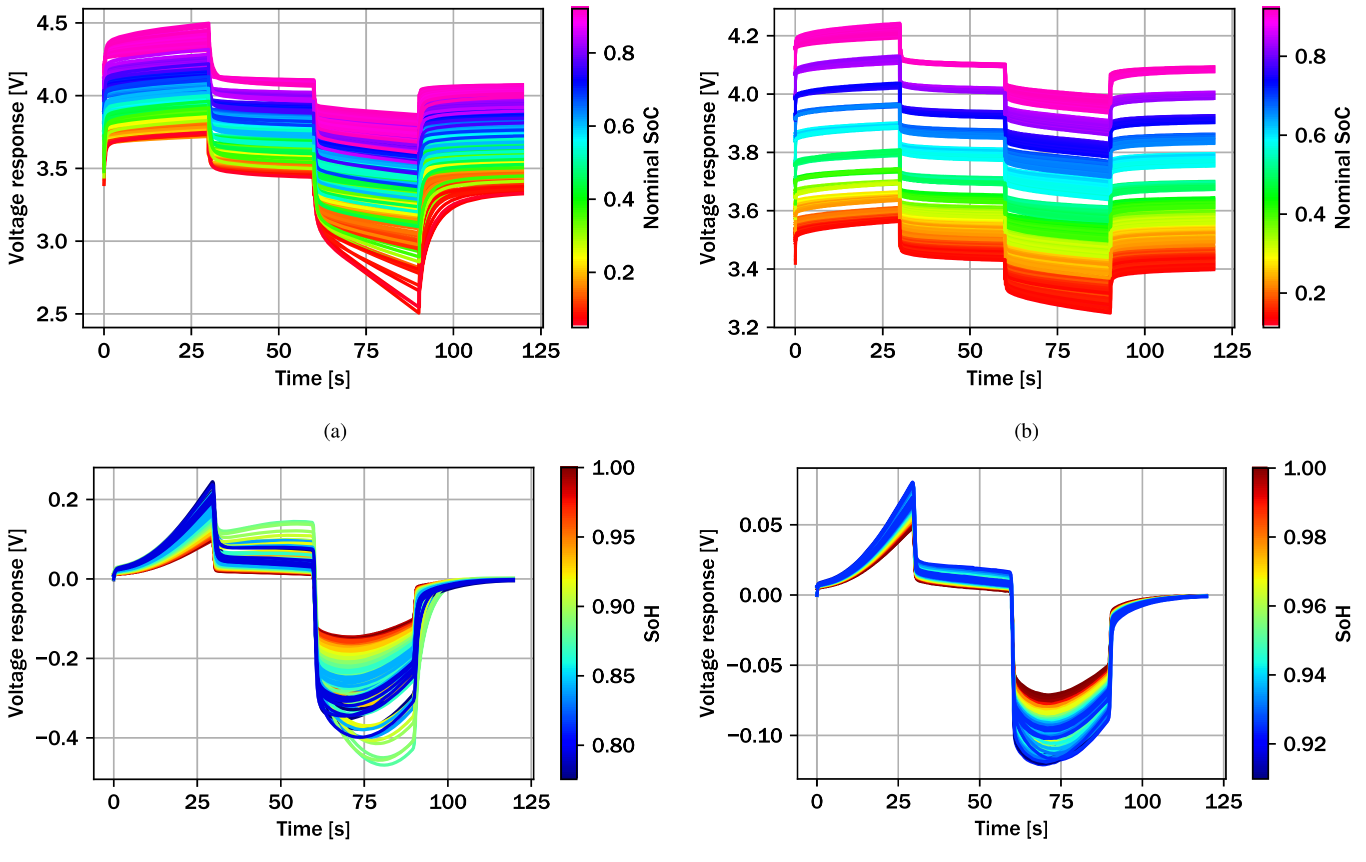

(a)

(b)

(c)

(d)

Fig. 2. Pulse data of cells degraded by S1 (left column) and S2 (right column) showing observed voltage color-coded by SoC (top row) and Hamming-windowed zero-mean voltage color-coded by SoH (bottom row).

We examine 363 unique combinations of SoC and SoH for stress factor 1, and 367 for stress factor 2, giving a total of 730 pulses for verification. Capacity checks are performed every 100 cycles using a 1/20 C-rate discharge from full. After the capacity check, pulses are applied from rest at various SoC similar to the galvanostatic intermittent titration technique (GITT) protocol [12]. The pulse voltages are shown in Figs. 2a and 2b, with the windowed voltage signals shown in Figs. 2c and 2d.

B. Verification with time-domain fitting

Validation of PIS is performed by analyzing the same pulse datasets in the time-domain with the CDD model. Since the Randles and CDD models theoretically model the same overpotentials, similar parameter trends are expected. Both models use an ohmic resistance, an RC-pair, and a diffusion component. While the CDD model operates in the time-domain and models the time-varying voltage, the Randles circuit operates in the frequency domain and models the frequency-varying impedance. Our aim is to show that the parameter trends in the CDD and Randles circuits are similar.

Parameters for the CDD model are obtained by fitting the overpotentials to pulse data in the time-domain, as detailed in [11]. The predicted output voltage $\hat{V}$ is given by the sum of the time-varying overpotentials,

$$\hat{V}(t) = V_{OC}(t) - V_s(t) - V_{ct}(t) - V_D(t) \tag{6}$$

where V_{OC} is the open-circuit voltage (OCV) and V_s, V_{ct}, and V_D are the solution, charge-transfer, and diffusion overpotentials. The terms $V_{OC}(t)$, $V_s(t)$, and $V_{ct}(t)$ are defined by the standard n^{th}-order resistor-capacitor (NRC) equations as listed in [25]. The diffusion overpotential is derived in [11] from the convolution of the diffusion state amplitude ζ with the unit impulse response $g_z(t)$,

$$V_D(t) = A_D \cdot \zeta(t) * g_z(t) \tag{7}$$

where A_D is the diffusion constant, also inverse-square proportional to the diffusion coefficient,

$$\frac{1}{A_D} = \frac{SF\sqrt{D\pi}}{2\beta v_M} \tag{8}$$

where $1/\beta$ is the maximum stoichiometric added lithium, S is the active surface area, and v_M is the molar volume of active material. Note the similarities with Eq. (4). Amplitude ζ is given by

$$\zeta(t) = \Big(i(t) - i(t - \Delta t)\Big)\nabla V_{OC}(t) \tag{9}$$

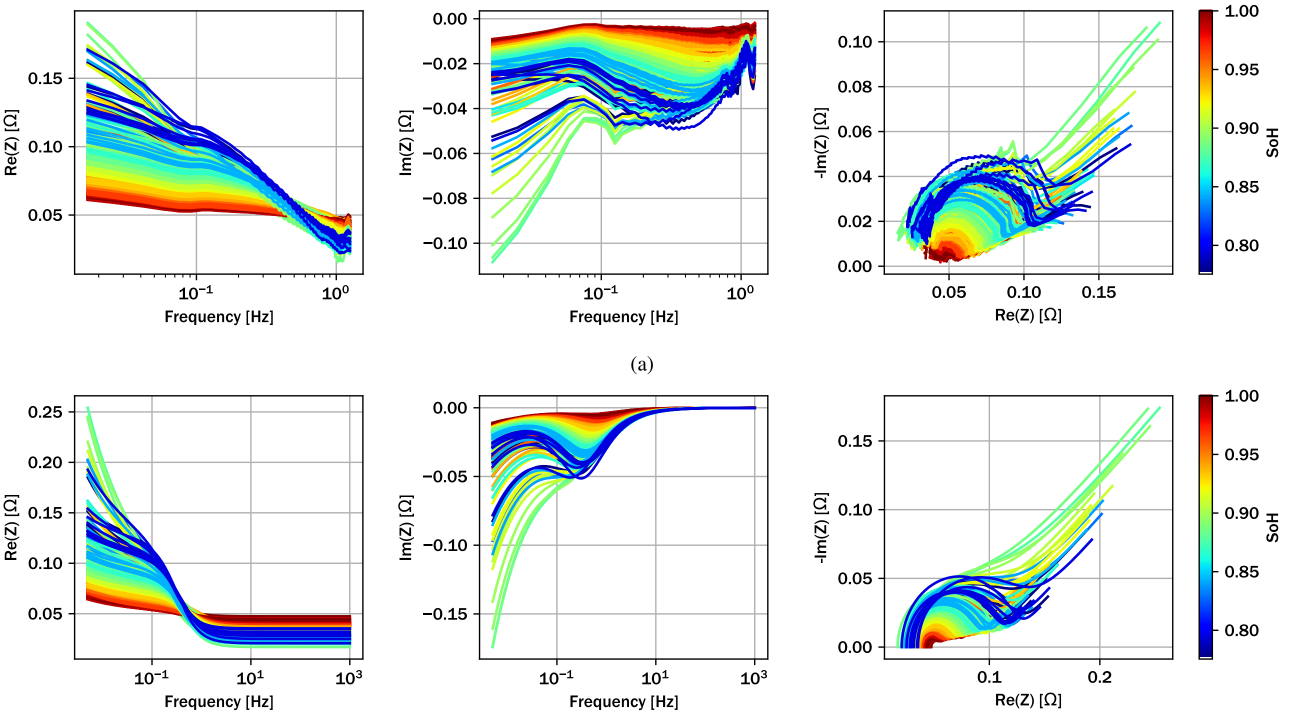

(a)

(b)

Fig. 3. Real (left), imaginary (middle); and Nyquist (right) impedance plots for S1, showing (a) Observed frequency-varying data and (b) Fitted impedance from the Warburg-1RC model with expanded frequency range.

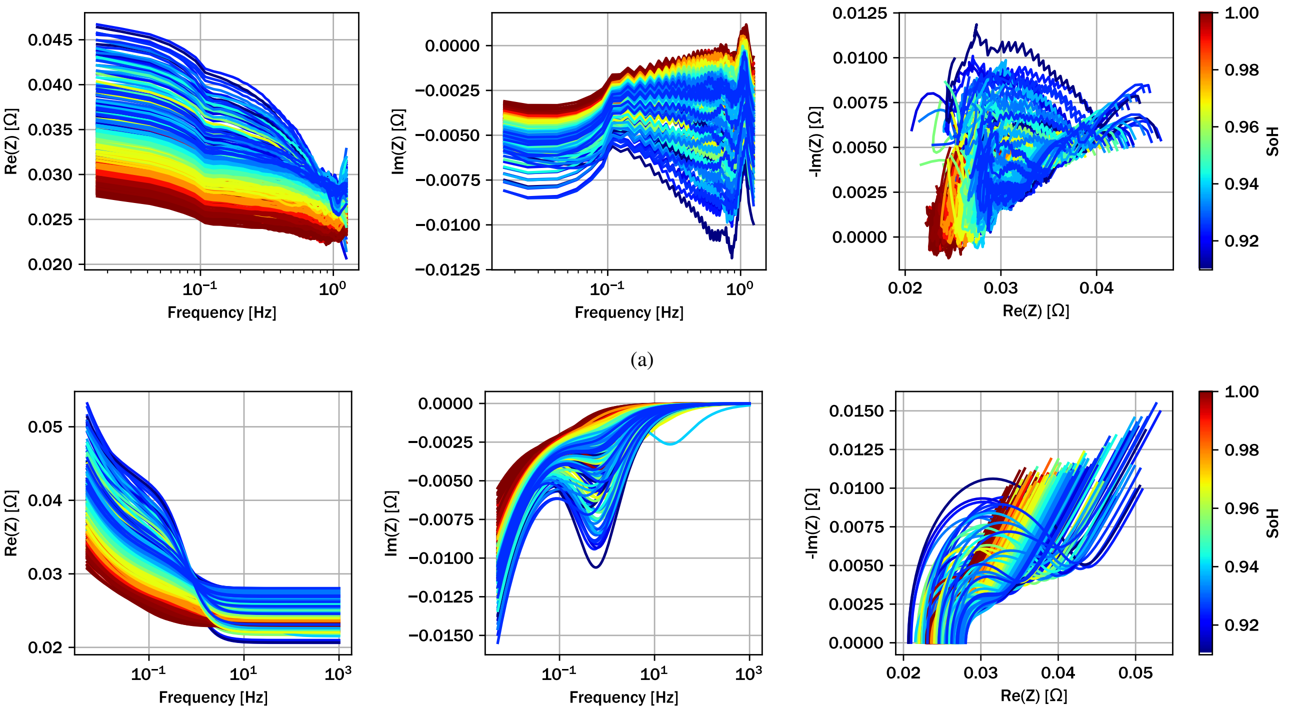

(a)

(b)

Fig. 4. Real (left), imaginary (middle); and Nyquist (right) impedance plots for S2, showing (a) Observed frequency-varying data and (b) Fitted impedance from the Warburg-1RC model with expanded frequency range.

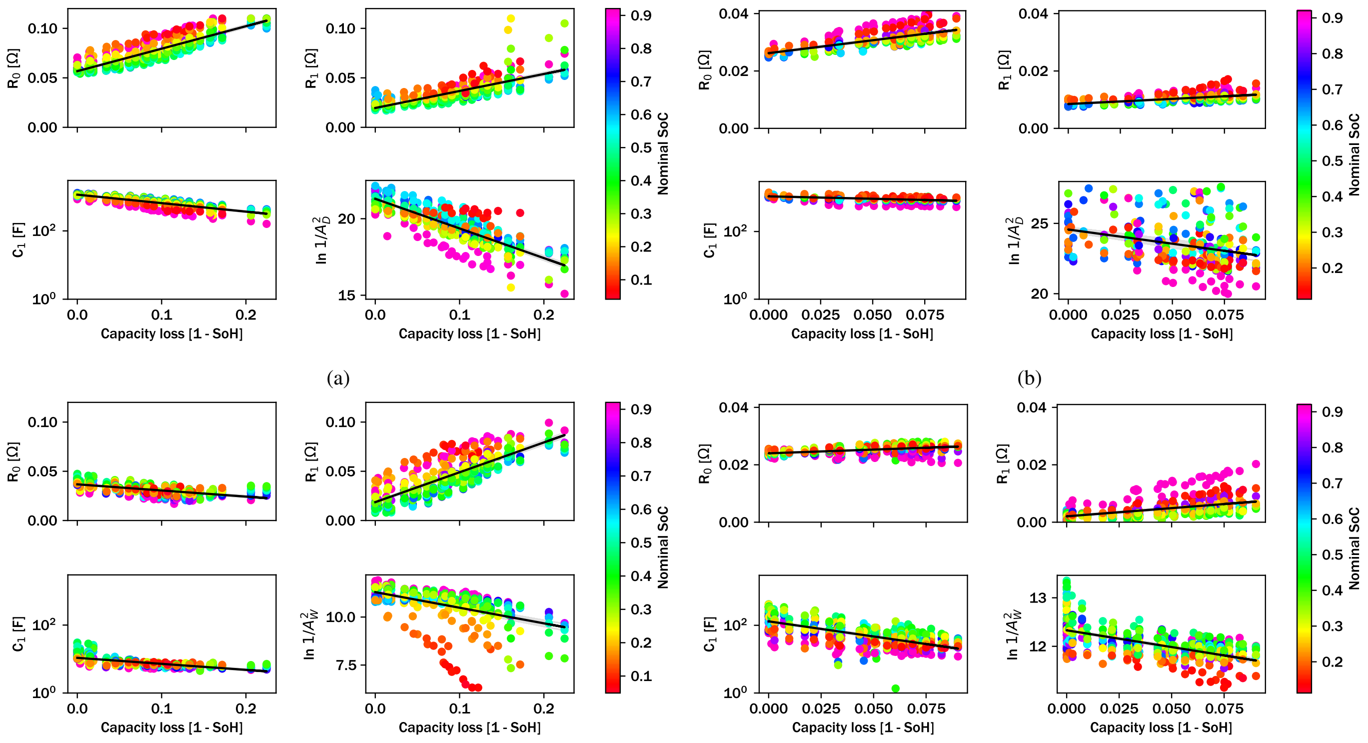

(a)

(b)

(c)

(d)

Fig. 5. Evolution of fitted parameters against capacity fade for S1 (left column) and S2 (right column) obtained using the CDD-1RC model on time-domain data (a)-(b) and the Warburg-1RC model on post-processing frequency data (c)-(d).

while the unit impulse response is given by

$$g_z(t) = \sqrt{t} - \sqrt{t - \Delta t} \tag{10}$$

Parameter identification is performed as above in Eq. (5), but the residuals and parameter vector are redefined as

$$\begin{aligned} r(k) &= V(t_k) - \hat{V}(t_k, \theta) \\ \theta &= (R_0 \quad R_1 \quad C_1 \quad A_D)^T \end{aligned} \tag{11}$$

and where V is the observed voltage response.

IV. RESULTS AND DISCUSSION

Observed and fitted Nyquist curves for S1 and S2 are shown in Figs. 3 and 4. Observed Nyquist curves for S1 are quite high quality in the low- to mid-range frequencies, as seen in the coherent semicircle. The low-frequency tail is clearly defined for S1, indicating that the 2-minute pulse sufficiently captures diffusion dynamics. As the SoH decreases, the semicircle width increases, as expected. In S2, the Nyquist curves are poorly defined. This may be attributed to the low magnitude of imaginary impedance, making it more sensitive to noise. Distortion therefore occurs because of the dominance of the real impedance.

At high frequencies there is more noise in the observed data. This is due to the relatively low sampling frequency of 10 Hz. By the Nyquist sampling theorem, this limits the maximum observable frequency component to 5 Hz. Despite this limit, the fitted curves can accurately reconstruct the data. This shows that fast PIS is a viable technique for analyzing the frequency-varying battery impedance.

Fitted curves are displayed with an expanded frequency range. Since the low- and mid-range frequencies are well-captured in the observed data, the fitted curves match the low- and mid-range frequencies well. At high-frequencies there is more uncertainty. Furthermore, the x-intercept decreases with SoH. As discussed above, this is because the fit extrapolates beyond the physically observable frequencies, creating a discrepancy with the real behavior. With a higher Nyquist sampling frequency, this issue can be avoided.

Parameter evolution of the CDD and Randles circuits is shown in Fig. 5. There are clear trends in the parameters of both models, and the two stress factors are highly distinguishable from each other. Resistances increase with capacity loss while the capacitance and the diffusion coefficient decrease exponentially. Parameters in S1 have higher magnitude and greater variation than S2 parameters, suggesting that S1 more severely degrades the LIB cells. The low impedance of S2, in particular, may explain the poorer quality of the Nyquist curves. Since the impedance is lower, it is more susceptible to noise in the frequency spectrum.

Both models exhibit similar trends in R_1, C_1, and D. This verifies the PIS results. Though the CDD model and Randles circuits have different formulations and aim to fit different types of data, the parameters are quantitatively and qualitatively linked. Thus we see that fast PIS offers an alternative to ECM modelling while linking the CDD with the Randles circuit.

There are discrepancies in the parameter trends caused by issues in the data collection and processing. For S1, the Randles R_0 does not increase with capacity loss. As noted above, this may be due to the insufficient sampling frequency of the pulse data, which would inadequately capture the solution overpotential. The diffusion parameters A_D and A_W are linked by very similar trends. The S1 Warburg impedance appears to have a low-SoC branch deviating from the trend. This could be explained by OCV variation in the pulse that is not explicitly considered in the Randles circuit. While OCV variation is negligible at most states of charge, at low SoC there is typically a large gradient in the OCV-SoC curve. This would then introduce a low-frequency dynamic into the Nyquist curve, explaining the low-SoC branch in the S1 diffusion trend.

V. CONCLUSION

We demonstrate the ability of PIS to obtain Nyquist curves using just 2 minutes of pulse perturbation data. PIS was analyzed using a wide range of LIB at multiple states and aging conditions. Though the quality of the Nyquist curves varies with the LIB stress factors, we show fast PIS is a useful method for verifying electrochemical overpotentials in experimental data. It extends time-domain EIS results from previous studies and provides an experimental link between the time-domain CDD overpotential ECM and the frequency-domain Randles circuit. Impedance spectroscopy and pulse perturbation are complementary tools for diagnosis and characterization of LIB cells.

One of the challenges of PIS is OCV variation in the pulse at low SoC levels. This would introduce low-frequency dynamics that could obfuscate results for the diffusion overpotential. A new frequency-domain OCV element could therefore be developed. Additionally, further work is needed to address the poor-quality Nyquist curves. Decreasing the time-domain sampling interval could allow high-frequency dynamics to be accurately captured. More advanced signal processing techniques can be used to improve the analysis. Finally, PIS can be compared with traditional impedance spectroscopy through further data collection.

REFERENCES

[1] J. S. Edge, S. O'Kane, R. Prosser, N. D. Kirkaldy, A. N. Patel, A. Hales, A. Ghosh, W. Ai, J. Chen, J. Yang, S. Li, M. Pang, L. B. Diaz, A. Tomaszewska, M. W. Marzook, K. N. Radhakrishnan, H. Wang, Y. Patel, B. Wu, and G. J. Offer, "Lithium ion battery degradation: what you need to know," *Phys. Chem. Chem. Phys.*, vol. 23, no. 8200, 2021.

[2] T. Kim, W. Song, D. Son, L. K. Ono, and Y. Qi, "Lithium-ion batteries: outlook on present, future, and hybridized technologies," *J. Materials Chem. A*, vol. 7, pp. 2942–2964, 2019.

[3] A. G. Li, , A. C. West, and M. Preindl, "Towards unified machine learning characterization of lithium-ion battery degradation across multiple levels: A critical review," *Appl. Energy*, vol. 316, no. 119030, 2022.

[4] A. G. Li, W. Wang, A. C. West, and M. Preindl, "Health and performance diagnostics in li-ion batteries with pulse-injection-aided machine learning," *Appl. Energy*, vol. 315, no. 119005, 2022.

[5] W. Choi, H. Shin, J. M. Kim, J. Choi, and W. Yoon, "Modeling and applications of electrochemical impedance spectroscopy (EIS) for lithium-ion batteries," *J. Electrochem. Sci. and Tech.*, vol. 11, no. 1, pp. 1–13, 2020.

[6] N. Meddings, M. Heinrich, F. Overney, J. Lee, V. Ruiz, E. Napolitano, S. Seitz, G. Hinds, R. Raccichini, M. Gaberscek, and J. Park, "Application of electrochemical impedance spectroscopy to commercial li-ion cells: A review," *J. Power Sources*, vol. 480, no. 228742, 2020.

[7] C. Pastor-Fernandez, K. Uddin, G. H. Chouchelamane, W. D. Widanage, and J. Marco, "A comparison between electrochemical impedance spectroscopy and incremental capacity-differential voltage as li-ion diagnostic techniques to identify and quantify the effects of degradation modes within battery management systems," *J. Power Sources*, vol. 360, pp. 301–318, 2017.

[8] U. Westerhoff, K. Kurbach, F. Lienesch, and M. Kurrat, "Analysis of lithium-ion battery models based on electrochemical impedance spectroscopy," *Energy Tech.*, vol. 4, pp. 1620–1630, 2016.

[9] A. Barai, K. Uddin, M. Dubarry, L. Somerville, A. McGordon, P. Jennings, and I. Bloom, "A comparison of methodologies for the non-invasive characterisation of commercial li-ion cells," *Progress in Energy and Combustion Science*, vol. 72, pp. 1–31, 2019.

[10] C. Pastor-Fernandez, T. F. Yu, W. D. Widanage, and J. Marco, "Critical review of non-invasive diagnosis techniques for quantification of degradation modes in lithium-ion batteries," *Renew. Sustain. Energy Rev.*, vol. 109, pp. 138–159, 2019.

[11] A. G. Li and M. Preindl, "Linear state-space modelling of the diffusion overpotential in li-ion batteries using a receding horizon," *Appl. Energy*, unpublished.

[12] W. Weppner and R. A. Higgins, "Determination of the kinetic parameters of mixed-conducting electrodes and application to the system li3sb," *J. Electrochem. Soc.*, vol. 124, no. 1569, 1977.

[13] J. R. Belt, "Battery test manual for plug-in hybrid electric vehicles," *Idaho National Lab, USA*, vol. 449, no. 227297, 2010.

[14] D. M. Bernardi and J. Y. Go, "Analysis of pulse and relaxation behavior in lithium-ion batteries," *J. Power Sources*, vol. 196, pp. 412–427, 2011.

[15] W. D. Widanage, A. Barai, G. H. Chouchelamane, K. Uddin, A. McGordon, J. Marco, and P. Jennings, "Design and use of multisine signals for li-ion battery equivalent circuit modelling. part 1: Signal design," *J. Power Sources*, vol. 324, pp. 70–78, 2016.

[16] H. Zappen, F. Ringbeck, and D. U. Sauer, "Application of time-resolved multi-sine impedance spectroscopy for lithium-ion battery characterization," *Batteries*, vol. 4, no. 64, 2018.

[17] N. Lohman, P. Wesskamp, P. Haussman, J. Melbert, and T. Musch, "Electrochemical impedance spectroscopy for lithium-ion cells: Test equipment and procedures for aging and fast characterization in time and frequency domain," *J. Power Sources*, vol. 273, pp. 613–623, 2015.

[18] B. Liebhart, L. Komsiyska, and C. Endisch, "Passive impedance spectroscopy for monitoring lithium-ion battery cells during vehicle operation," *J. Power Sources*, vol. 449, no. 227297, 2020.

[19] A. Savitzky and M. J. E. Golay, "Smoothing and differentiation of data by simplified least squares procedures," *Anal. Chem.*, vol. 36, no. 8, 1964.

[20] J. Huang, "Determination of diffusion coefficients using impedance spectroscopy data," *Electrochimica Acta*, vol. 281, pp. 170–188, 2018.

[21] T. Q. Nguyen and C. Breitkopf, "Determination of diffusion coefficients using impedance spectroscopy data," *J. Electrochem. Soc.*, vol. 165, no. 14, 2018.

[22] D. M. Bernardi and I. Lelidis, "Analysis of warburg's impedance and its equivalent electric circuits," *Phys. Chem. Chem. Phys.*, vol. 19, no. 24934, 2017.

[23] S. Saxena, D. Roman, V. Robu, D. Flynn, and M. Pecht, "Battery stress factor ranking for accelerated degradation test planning using machine learning," *Energies*, vol. 14, no. 723, 2021.

[24] Y. Preger, H. M. Barkholtz, A. Fresquez, D. L. Campbell, B. W. Juba, J. Roman-Kustas, S. R. Ferreira, and B. Chalamala, "Degradation of commercial lithium-ion cells as a function of chemistry and cycling conditions," *J. Electrochem. Soc.*, vol. 167, no. 120532, 2020.

[25] A. G. Li, K. Mayilvahanan, A. C. West, and M. Preindl, "Discrete-time modeling of li-ion batteries with electrochemical overpotentials including diffusion," *J. Power Sources*, vol. 500, no. 229991, 2021.